RESEARCH ARTICLE
PLANETARY SCIENCES

Earth and Planetary Physics
9: 1113–1124, 2025
doi: 10.26464/epp2025070

The density distribution and 58.4 nm radiation intensity of interstellar helium in the heliosphere: a model simulation

JiaLing Lyu[1,2], ChongJing Yuan[1,2*], Fei He[1,2], and BeiLi Ying[3]

[1]Key Laboratory of Planetary Science and Frontier Technology, Institute of Geology and Geophysics, Chinese Academy of Sciences, Beijing 100029, China;

[2]College of Earth and Planetary Sciences, University of Chinese Academy of Sciences, Beijing 100049, China;

[3]Key Laboratory of Dark Matter and Space Astronomy, Purple Mountain Observatory, Chinese Academy of Sciences, Nanjing 210023, China

Key Points:

- Studying the absorption and scattering effects of the interstellar medium is of significance in interpreting stellar EUV emissions and understanding the evolution of stars.
- This work establishes a model of the penetrating interstellar helium density distribution in the heliosphere and the corresponding 58.4 nm radiation intensity.
- Our results facilitate the EUV full-sky survey of Queqiao-2, the relay satellite of the China's Lunar Exploration Program.

Citation: Lyu, J. L., Yuan, C. J., He, F., and Ying, B. L. (2025). The density distribution and 58.4 nm radiation intensity of interstellar helium in the heliosphere: a model simulation. *Earth Planet. Phys.*, *9*(6), 1113–1124. http://doi.org/10.26464/epp2025070

Abstract: Research on the interstellar medium and its interaction with the solar system constitutes a significant topic in planetary physics. As the Sun traverses the local interstellar cloud, interstellar neutrals penetrate the heliosphere, forming the interstellar wind, and scattering solar extreme ultraviolet (EUV) emission lines. The intensity of the scattered radiation provides an indicator of the characteristic parameters of the interstellar wind, crucial for characterizing the heliosphere, the interstellar medium, and the evolution of the solar system. Meanwhile, a powerful method for studying stellar evolution is investigating the EUV emissions of stars. The only ongoing mission conducting an EUV full-sky survey is the relay satellite Queqiao-2. Due to the strong absorption of the interstellar medium at EUV wavelengths, modelling is essential to any study of these influences. In this study, we reviewed classical modelling methods for the density distribution of the interstellar helium atoms in the heliosphere, and the corresponding 58.4 nm radiation intensity. We established distinct density and intensity models for different orbital positions of Earth's revolution. We found that when the Earth enters the helium focusing cone in the downwind region, both the helium density and the 58.4 nm radiation intensity increase rapidly, with the temperature effect being particularly important. The radiation intensity in the downwind direction can be 170 times that of the upwind direction. Some negligible factors were omitted for simplicity, such as the effects of the solar line width and Doppler shift. Our research can serve as an aid to the interpretation of the EUV observations in the full-sky survey conducted by Queqiao-2.

Keywords: Interstellar wind; heliosphere; interstellar helium atoms; resonantly scattered radiation

1. Introduction

The Sun and the surrounding interstellar medium are of fundamental interest to planetary physics and astrophysics. Over the past several million years, the solar system has traversed the Local Bubble: a very low-density region of Gould's Belt near the inner rim of the Orion Arm of the Milky Way Galaxy. The Sun is now embedded in a tenuous, warm, partially ionized interstellar cloud, the Local Interstellar Cloud (LIC), which flows from the Scorpius-Centaurus star-forming region (Frisch, 2006). Similar to the interaction between the Earth's magnetosphere and the solar wind, the Sun's magnetic fields carve a tailed bubble-like region—the heliosphere—within the LIC, and mutually interacts with the interstellar wind (ISW), which mainly contains of particles, gas, and dusts that form the local interstellar medium (LISM). The heliopause blocks the charged particles in the ISW from entering the heliosphere, but not the neutrals, which mainly consists of hydrogen, helium, and oxygen (Grava et al., 2018). These atoms resonantly scatter solar EUV emission lines at 121.6 nm (H I Lyman α), 58.4 nm (He I), and 83.4 nm (O I), respectively, which are detectable by telescopes and spectrometers.

The study of the scattering of solar EUV radiation by interstellar neutral atoms is significant for understanding the heliosphere–LISM interaction, as well as the activities and evolutionary history of the solar system. The characteristic parameters of ISW, such as the flow velocity, direction, temperature, and density, constrain the size, shape, and composition of the heliosphere. Among these, the flow velocity strongly influences the heliospheric interface structure (Lallement and Bertaux, 2014; Spitzer et al., 2024). Determining the above parameters is not only an effective way to learn the physics of the heliosphere and quantify its interaction

First author: J. L. Lyu, lvjialing@mail.iggcas.ac.cn
Correspondence to: C. J. Yuan, chjyuan@mail.iggcas.ac.cn
Received 24 JAN 2025; Accepted 23 APR 2025.
First Published online 17 JUL 2025.

with the LISM, but also helps to understand the processes occurring within the LISM. Observing the 121.6 nm and 58.4 nm radiation scattered by interstellar hydrogen and helium is one of the most important approaches to deriving the characteristic parameters of the ISW (e.g., Ajello, 1978; Nakagawa et al., 2008; Grava et al., 2018). Other important approaches include in situ direct sampling of helium atoms (e.g., Witte et al., 1992; Witte, 2004; McComas et al., 2015), as well as pickup ion measurements in the downwind helium focusing cone (e.g., Möbius et al., 1985; Gloeckler et al., 1998). Despite numerous theoretical and observational studies of the ISW, controversies persist regarding the flow direction and the helium "warm breeze"—a discrepancy arising from the different measurement techniques used by IBEX (Interstellar Boundary Explorer) and Ulysses, which is no longer operating. IBEX detects neutral helium atoms entering the heliosphere through energetic neutral atom imaging (Kubiak et al., 2014), while Ulysses measured in-situ ionized helium within the solar wind (Witte, 2004). The inconsistency in observations of flow direction sparked debate: At first, Frisch et al. (2013, 2015) proposed temporal variations as the cause, whereas Lallement and Bertaux (2014) attributed it to instrumental biases. Later, IBEX identified an additional helium population in the ISW, the aforementioned "warm breeze", which is a secondary stream of interstellar helium atoms with higher thermal velocities (~11 km s^{-1}) compared to the primary population (Kubiak et al., 2014). Yet neither this component nor temporal variations were confirmed by the Lunar Reconnaissance Orbiter (Grava et al., 2018). Additionally, a more recent study with the Advanced Composition Explorer (ACE) spacecraft revealed no significant shift in the inflow direction over an 11-year solar cycle (Spitzer et al., 2024). The resolving of these controversies has critical implications for ISW dynamics. Precise determination of the flow direction and the "warm breeze" properties is essential for modeling the heliosphere's interaction with the interstellar medium, itself a key factor in understanding the solar system's galactic environment (McComas et al., 2015). It can be concluded that more coherent observations with higher temporal and spatial resolution are crucial for future studies, and that revisiting old models and data can sometimes provide new insights.

Studying the solar EUV radiation scattered by the interstellar neutrals is of great importance for understanding the evolution of stars and their planetary systems. The EUV spectrum of a star reflects the composition, abundance, and radiation-generating mechanisms of the star (Craig et al., 1997). It also reflects the structure, parameters, age, and activity level of the star (Craig et al., 1997; Johnstone et al., 2021), as well as the evolution of the atmospheres of its planets (Drake et al., 2020; Johnstone et al., 2021). Since the beginning of the Space Age, there have been only two satellites capable of surveying the EUV emissions of extrasolar sources. One of them is the Extreme Ultraviolet Explorer (EUVE) satellite, which operated from 1992 to 2001, and established an atlas of EUV spectra from stellar sources (Craig et al., 1997). The sole ongoing mission to survey EUV emissions is the relay satellite included in Phase IV of China's Lunar Exploration Program, Queqiao-2, which conducts a full-sky survey in the EUV band. However, the interstellar neutral helium distributed along the line of sight (LOS) of the satellite's observation strongly absorbs the EUV emissions of extrasolar stars. For instance, the observations of EUVE showed that the lack of the 30.4 nm He II emission of an early-type star, β Canis Majories, indicated the existence of high interstellar neutral helium column density along the LOS (Craig et al., 1997). Thus, understanding the ISM absorption effect is essential for interpreting EUV observations. The heliosphere is a giant natural laboratory for such studies, the scattered 58.4 nm radiation serving as a probe of interstellar neutral helium, enabling investigations into its properties and absorption effects on stellar EUV emissions.

To facilitate the EUV-wavelength full-sky survey of the EUV camera onboard Queqiao-2 (He F et al., 2025; He LP et al., 2025), this work aims to study the 58.4 nm radiation of interstellar helium in the heliosphere by building a density model of helium and calculating the corresponding radiation intensity. The interstellar helium atom is the primary neutral component of the gases in the vicinity of the Earth, because it experiences strong gravitational force and negligible solar radiation pressure, due to its larger mass and higher ionization potential compared to hydrogen. In Section 2, we review the classic helium density models of Feldman et al. (1972) and Blum et al. (1975), then build the model for all-sky He I 58.4 nm radiation distribution. Our model results are shown in Section 3, and the discussion and conclusions are presented in Section 4.

2. Modelling Methods

The trajectories and density distribution of the incoming interstellar helium atoms were first analyzed by Feldman et al. (1972). Their results, named the "Feldman approximation", especially considered the gravitational focusing effect and temperature in the downwind region of the ISW. Johnson (1972) subsequently established a more comprehensive model of helium density distribution in the ecliptic plane, without considering the temperature of the ISW. Later, Paresce and Bowyer (1973) advanced Johnson's calculations to include all possible directions of observation. Finally, Blum et al. (1975) modified Johnson's density model, and also derived an interpolation formula for Feldman's approximation, which has become the most commonly used model, called the "BPW model". A number of previous studies derived the backscattered 58.4 nm radiation intensity distribution from helium density (Paresce and Bowyer, 1973; Ajello, 1978; Wu FM and Judge, 1979). All of the aforementioned calculations will be revisited and discussed in this section.

2.1 The Density Model of Interplanetary Helium

Each interstellar helium atom follows a hyperbolic trajectory in a two-dimensional plane (the ecliptic plane) with the Sun as its focus (Feldman et al., 1972; Johnson, 1972). They can be treated as free particles due to a very large mean free path for atom–atom collisions (~10^3 astronomical unit, AU) (Thomas, 1978; Johnson, 1972). The dominant loss mechanism for helium atoms is photoionization (Rucinski and Fahr, 1989). Since the observed ecliptic latitude of the interstellar wind direction is very low (~5°, Swaczyna et al., 2023), we assume that the velocity vector of the wind is located within the ecliptic plane. The coordinate system in this section is a heliocentric polar coordinate system with the distance from the Sun r, and the angular distance from the upwind direction θ. Each point $P(r, \theta)$ in space is the intersection of two helium orbits: the direct orbit and the indirect orbit (Johnson, 1972; Blum et al., 1975). The latter bypasses the Sun, while the former does not (see Figure 1a).

2.1.1 The downwind region

As a result of the gravitational focusing effect of the Sun, helium atoms congregate in the downwind region, which is defined as a cone with an axis parallel to the downwind direction, and an aperture angle δ_c (or the critical angle). The high density in the cone causes enhanced temperatures and 58.4 nm radiation intensity (discussed in Section 2.2), therefore the thermal velocities of helium atoms are important inside the cone. According to the Feldman approximation (Feldman et al., 1972), the number density along the downwind axis ($\theta = \pi$) is given by

$$n(r,\pi) = N\sqrt{\frac{\pi GMm(1-\mu)}{kTr}}\exp\left(-\frac{\pi r_i}{\sqrt{\frac{2r}{C}}}\right), \tag{1}$$

with the effective penetration depth

$$r_i = \frac{\beta_0 r_e^2}{V},$$

and

$$C = \frac{V^2}{(1-\mu)GM},$$

where N is the helium number density at infinity, μ is the ratio of the force of radiation pressure on each atom to that of gravity (for helium, $\mu \sim 0$), r_e is the distance between the Sun and the Earth, and $\beta_0 = 0.03 \times 10^{-7}$ s^{-1} is the loss coefficient at $r = r_e$ (Johnson, 1972). G, M, m, k, T and V are the gravitational constant, the mass of the Sun and a helium atom, the Boltzmann constant, the temperature and velocity of the inflow ISW, respectively.

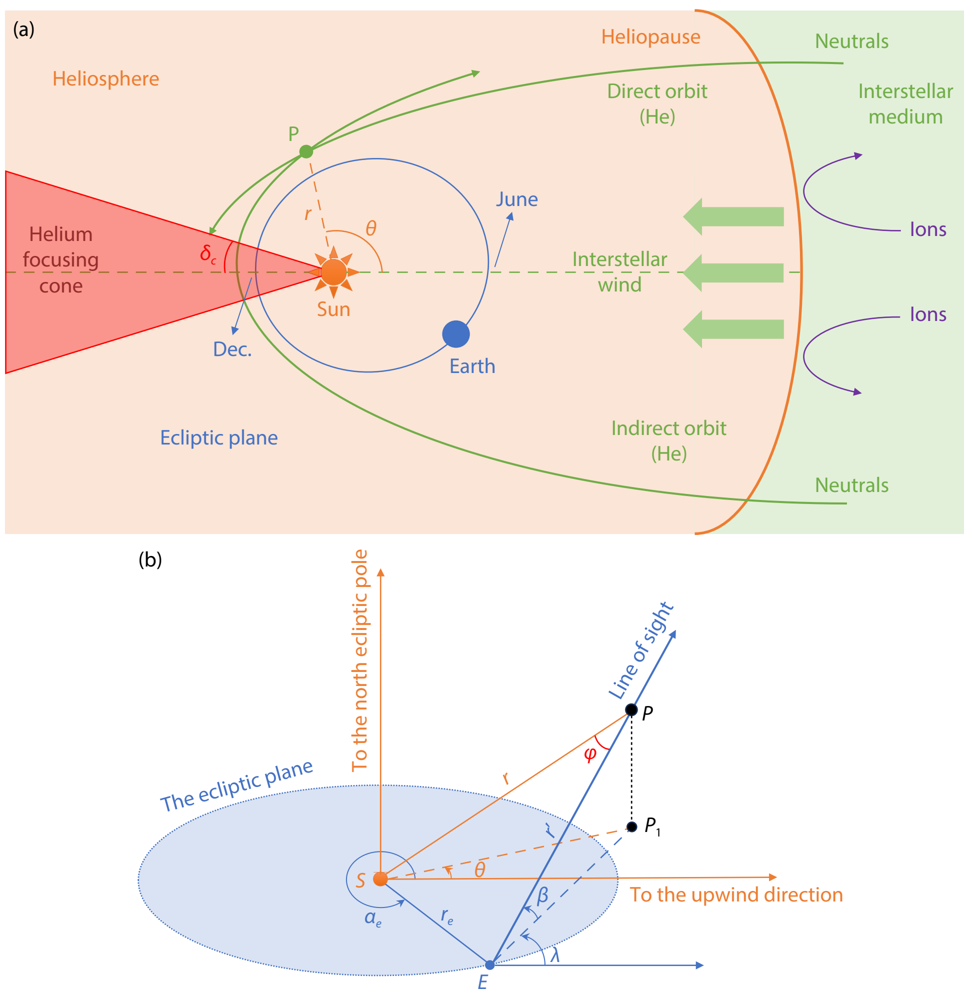

Figure 1. (a) A schematic diagram of the interactions between the heliosphere and the interstellar space. The heliosphere is shown as the orange region on the left, while the ISM is shown as the light green region on the right, parted by the heliopause, which is shown as the bold orange line. The heliopause blocks interstellar ions (the purple arrowed lines) from entering the heliosphere, but does not block the neutrals (the green arrowed lines). The two trajectories of interstellar helium and the heliocentric polar coordinate (r, θ) are shown in the diagram. The Earth and its orbit are shown as the blue dot and elliptic circle. The downwind focusing cone of the helium is shown as the red shaded cone region, with an aperture angle δ_c. The diagram is in the ecliptic plane and not to scale. The diagram is adapted from Spitzer et al. (2024). (b) A diagram of the coordinate systems. The letters "S", "E", and "P" represent the Sun, the Earth, and the observing point, respectively, and "P_1" is the projection of point "P" to the ecliptic plane. We present our results in the ecliptic coordinates (r', λ, β), where r', λ, and β are the geocentric distance, the ecliptic longitude, and latitude, respectively (Note that the primary direction of the ecliptic longitude points in the anti-parallel direction of the ISW, not towards the vernal equinox). α_e is defined as the angle between the upwind direction and the Sun-Earth line, r_e is the distance between the Sun and Earth (1 AU), and φ is the polar phase angle of the scattering atom.

Introducing an angle $\delta = |\pi - \theta|$, if $\delta < \delta_c = 3\sqrt{\frac{kT}{2\pi m V^2}}$ (i.e. considering a point within the focusing cone), then the number density is given by

$$n(r,\theta)_{\delta<\delta_c} = n(r,\pi)\left[1 - \frac{2\pi m V^2}{27kT}\delta^2\right]. \tag{2}$$

Feldman's calculations were proved to provide a good approximation of the helium density within a distance of 1 AU from the Sun (Blum et al., 1975; Ajello, 1978), but not over longer distances, yielding a vanishing density along the downwind axis when the relative density at infinity should be 1. This problem was reconsidered by Blum et al. (1975), and the details are presented in Appendix A1. Nevertheless, the discrepancies between the Feldman approximation and BPW's modification are acceptable in this paper, given our sole focus on distances that do not exceed 10 AU from the Sun (detailed comparisons are provided in Appendix A1).

2.1.2 The "general case" and upwind direction

The helium density distribution in the entire ecliptic plane was first derived by Johnson (1972) (see Appendix A2 for details). Johnson's calculation where subsequently improved by Blum et al. (1975) further improved to include the electron ionization effect as well as the focusing or defocusing effects. The revised expression for helium density distribution is:

$$n(r,\theta)_{\delta>\delta_c} = N\sum_{j=1}^{2} n_j^*(r,\theta)\exp\left[-\frac{r_e^2}{\tau_e}\left(\frac{\theta_j}{Vp_j} + \frac{1}{v_{sw}r}\frac{\tau_e}{\tau_e^{(c)}}\right)\right], \tag{3}$$

where τ_e or $\tau_e^{(c)}$ is the lifetime of helium atoms at 1 AU ($\tau_e^{(c)}$ when the corpuscular fluxes are included (Blum et al., 1975)), v_{sw} is the solar wind speed,

$$n_j^*(r,\theta) = \frac{1}{\frac{r}{p_j}|\sin\theta_j|\left(2 - \frac{r}{p_j}\sin\theta_j\right)}, \tag{4}$$

and

$$p_j = \frac{1}{2}r\sin\theta_j\left(1 + (-1)^{j+1}\sqrt{1 + \frac{4}{rC(1+\cos\theta)}}\right) \tag{5}$$

are the angular momenta of the direct orbit ($j = 1$) and the indirect orbit ($j = 2$), where θ is used without index as $\cos\theta_1 = \cos\theta_2$. The term $n_j^*(r,\theta)$ expresses the focusing or defocusing effects due to the trajectorial geometry; the additional term $\exp\left[-\frac{r_e^2}{\tau_e}\left(\frac{1}{v_{sw}r}\frac{\tau_e}{\tau_e^{(c)}}\right)\right]$ is only important for small distance r, i.e. when the atoms penetrate into the solar system (closer to the Sun than Earth), which is not taken into account in this work which assumes the observer to be located on Earth.

Particularly for the upwind direction, the BPW model gives

$$n(r,0) = \frac{1}{2}N\left(1 + \sqrt{1+\frac{2}{rC}} - \sqrt{\frac{1}{rC(rC+2)}}\right)\exp\left(-\frac{2r_e^2}{\tau_e V\left(1+\sqrt{1+\frac{2}{rC}}\right)r}\right). \tag{6}$$

Note that only the direct orbit ($j = 1$) is included, because the atoms cannot encircle the Sun, and the orbit in this case is oriented in a straight line toward the Sun. The lifetime of the interstellar helium atoms is chosen to be $\tau_e = 1.6\times10^7$ s, as this value was the "best fit" for the Mariner 10 data (Ajello, 1978).

All processes considered in this paper are linear with respect to the interstellar density (N) (Blum et al., 1975), therefore the number of helium atoms in the heliosphere can be evaluated by a dimensionless number: the relative number density n_{rel}, given by

$$n_{rel}(r,\theta) = \frac{1}{N}n(r,\theta). \tag{7}$$

2.2 The Intensity Model of 58.4 nm Radiation

Given the density distribution of helium, the resonantly scattered radiation intensity I in Rayleigh (1 Rayleigh = $\frac{10^6}{4\pi}$ photons cm^{-2} s^{-1} sr^{-1}) at 58.4 nm along a LOS can be calculated from (Thomas, 1978; Paresce et al., 1973; Ajello, 1978)

$$4\pi I(\lambda,\beta) = \int_0^\infty n(s)\,p[\varphi(s)]\,g(s)\,ds, \tag{8}$$

where λ and β represent the pointing direction on the celestial sphere in ecliptic longitude and latitude (see Appendix B for coordinate transitions), respectively; s is the distance along the LOS measured from the observer, and $p[\varphi(s)]$ is the phase function for the scattering (Ajello, 1978), which has a form of

$$p[\varphi(s)] = \frac{3[1+\cos^2\varphi(s)]}{4}, \tag{9}$$

at a scattering phase angle

$$\varphi(s) = \arccos\left(\frac{r^2 + r'^2 - r_e^2}{2rr'}\right), \tag{10}$$

where r' is the distance from Earth. The medium is assumed to be optically thin and only scatters once (Johnson, 1972). The g-factor, $g(s)$, or scattering rate, is a very important parameter in the calculation of radiation intensity, defined as the number of photons scattered per second, relating the radiation intensity to the column density of the scattering atoms along the LOS (Thomas, 1978). A simple form of the g-factor is used in this paper (Ajello, 1978):

$$g(s) = g_e\left[\frac{r_e}{r(s)}\right]^2, \tag{11}$$

where g_e is the g-factor value at 1 AU and $g_e = 1.62\times10^{-5}$s^{-1} (Ajello, 1978). Thus $g(s)$ in this form is a function only of heliocentric distance. However, since the solar line width at 58.4 nm is comparable with the Doppler shift from the solar line center of the helium atoms, it is necessary to carefully evaluate the effects of different solar line widths and Doppler shift for accuracy (Ajello, 1978). The thermal velocity dispersion of atoms and ions in the solar atmosphere causes Doppler shifts, and results in a broadening of the solar spectral line, described by the "solar line width". In this study the term "Doppler shift" refers to the shift from the solar line center produced by the heliocentric radial velocities of the interstellar helium atoms. For each point in space, the radial velocity distribution of the atoms determines the Doppler broadening of the line, which further determines the absorption rate of solar lines by the interstellar atoms (Wu FM and Judge, 1979), and affects the value of the scattered intensity. Further discussion are shown in Appendix C.

3. Results

3.1 Helium Density and Emissivity Distribution: the Sun's Perspective

We utilized the Feldman approximation (Equations (1) and (2) for the downwind region) and the BPW's modification (Equations (3)–(7) for other directions) to calculate the relative number density of interstellar helium atoms in the ecliptic plane, with the Sun as the center. The parameters of the interstellar wind were chosen as a velocity V = 20 km s^{-1} and a temperature T = 15,000 K, as initially measured by Mariner 10 (Ajello, 1978). These parameters have remained relatively stable over the intervening decades (Swaczyna et al., 2023). In Figure 2, we plot a contour of the helium density within a few AUs of the Sun. The red dashed circle and the blue dashed line represent the Earth's orbit and the edge of the focusing cone, respectively.

Figure 2 shows that the helium densities within the focusing cone are higher than those in other regions. At the same heliocentric distance r, the closer to the downwind axis (i.e. $\theta \to 180°$), the denser the helium gets; at the same polar angle θ in the focusing cone, the closer to the Sun, the denser the helium gets, while in other directions the situation is the opposite. The highest density appears in the downwind axis near the Sun. This discrepancy arises from the pronounced impact of solar gravitational focusing and the temperature effect in the downwind region, whereas in other directions, atoms are more susceptible to loss through photoionization.

The temperature effect in this study refers to the thermal motion of helium atoms due to the temperature of the ISW. The thermal velocity dispersion of the interstellar neutral helium atoms spreads the atom trajectories within the gravitational focusing cone. It determines the density gradient of helium atoms, which in turn affects their scattering of the solar EUV radiation. This effect is particularly important inside the cone, because it prevents infinite densities that would appear at the downwind axis when the neutral helium is treated as a cold gas without considering the atomic thermal motion (see Appendix A2 for details). Different temperatures affect the value of the aperture angle of the focusing cone and the maximum of the density. For a fixed bulk velocity, the lower the temperature is, the smaller the angle is, but the larger the maximum density becomes. It can be inferred that a lower ISW temperature leads to a more compressed helium focusing cone. For T = 15,000 K and V = 20 km s^{-1} in this paper, the aperture angle δ_c = 19.14°, and the maximum relative number density is 4.66.

The column emissivity of interstellar helium can be calculated from

$$\varepsilon(s) = n(s) \cdot g(s) \tag{12}$$

in photons cm^{-3} s^{-1}, defined as the number of photons scattered per second per unit space. The results are shown in Figure 3.

Based on Figure 2, Figure 3 demonstrates that the emissivity increases significantly when approaching the Sun from all directions, as the g-factor is inversely proportional to the square of the heliocentric distance. Note that the shape of the distribution is elongated along the downwind axis, suggesting that $n(s)$ has a greater influence on $\varepsilon(s)$ in the downwind region.

3.2 Helium Density Distribution and 58.4 nm Radiation Intensity: Earth's Perspective

Having computed the helium density distribution in the ecliptic plane within heliocentric coordinates, the corresponding distribution in geocentric coordinates can be derived through coordinate translation. The three-dimensional distribution within the heliosphere can then be obtained by rotating these coordinates, as interstellar helium atoms exhibit cylindrical symmetry with respect to the inflow direction of the ISW (Blum et al., 1975) (see Appendix B for details). Given the density distributions and the geometric relations of scattering, the intensity of the radiation scattered by interstellar helium atoms at 58.4 nm can be calculated

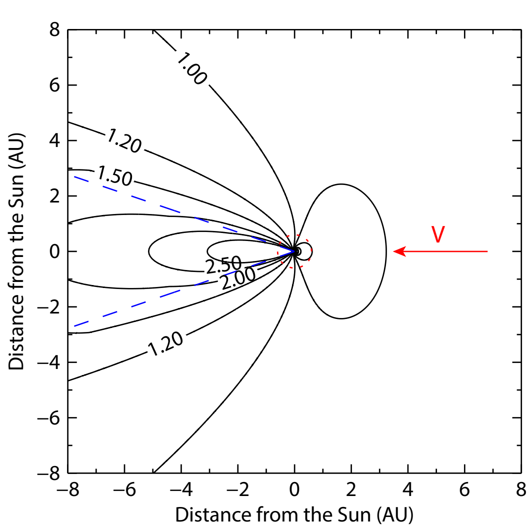

Figure 2. The relative number density distribution of interstellar helium atoms in the ecliptic plane in a heliocentric polar coordinate system. The red arrow (parallel to the horizontal axis) and the letter "V" represent the direction of the inflow interstellar wind.

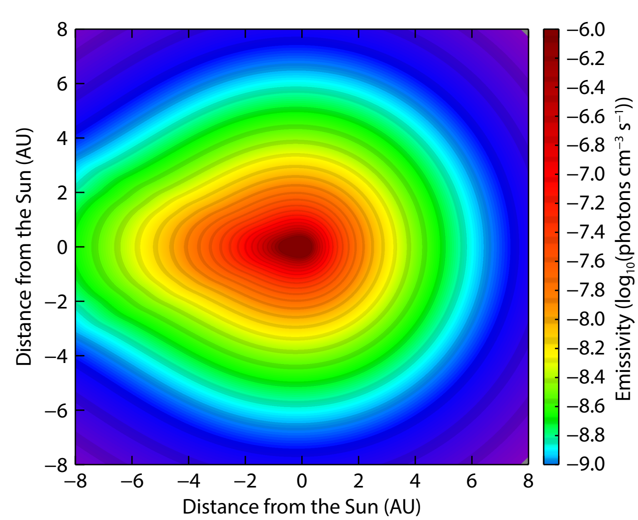

Figure 3. The column emissivity of 58.4 nm radiation in the ecliptic plane in heliocentric polar coordinate system, in the units of $\log_{10}\left(\text{photons cm}^{-3}\text{s}^{-1}\right)$.

from Equations (8)–(11). In this section, we first present the helium density distribution in the ecliptic plane in geocentric polar coordinates (Figure 4), then the ecliptic longitudinal and latitudinal distributions of the radiation intensity at 58.4 nm (Figure 5), and finally the all-sky maps of the intensities (Figure 6). As shown in Figure 1b, the angle between the upwind direction

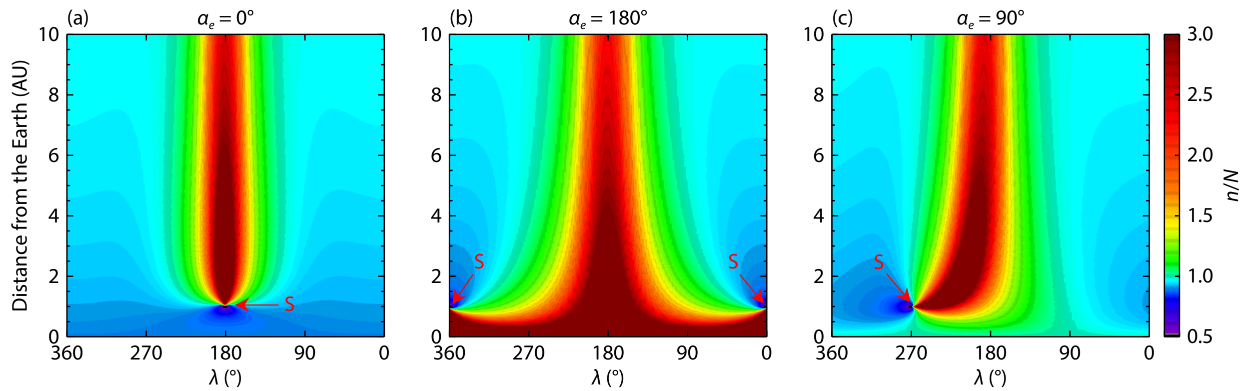

Figure 4. The relative number density distribution of helium, with the observer located on the Earth, when the Earth is on the upwind direction (a), the downwind direction (b), and the perpendicular direction (c). The horizontal axis represents the ecliptic longitude (see Figure 1 b) of the directions of the LOS, and the vertical axis represents the heliocentric distance. The color scale corresponds to the relative number density of helium (n/N, unitless), where n is the local number density and N is the value at infinity. The letter "S" and the red arrow indicate the Sun.

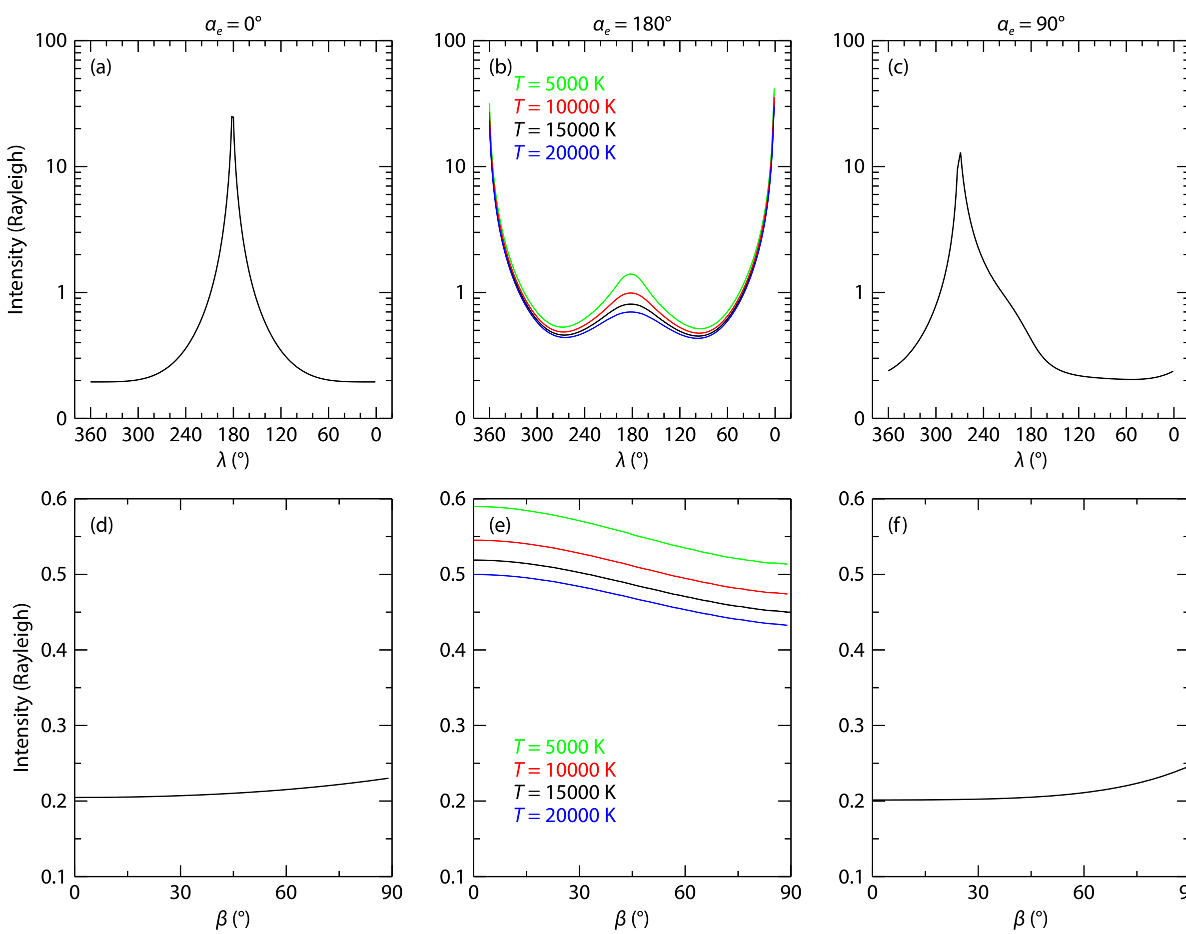

Figure 5. The longitudinal (panels (a–c), $\beta = 0°$) and latitudinal (panels (d–f), $\lambda = 70°$) distribution of He I 58.4 nm radiation intensity observed from Earth. Panels (a) and (d) show the Rayleigh intensity where $\alpha_e = 0°$, panels (b) and (e) are for $\alpha_e = 180°$, and panels (c) and (f) are for $\alpha_e = 90°$. In the $\alpha_e = 180°$ case, we plotted the results under different ISW temperatures: green lines for 5000 K, red lines for 10,000 K, black lines for 15,000 K, and blue lines for 20,000 K. The parameters we ultimately used are still $V = 20$ km s^{-1} and $T = 15{,}000$ K. The horizontal axes in panels (a–c) and panels (d–f) represent the ecliptic longitude λ and latitude β (see Figure 1b) of the directions of LOS, respectively. The vertical axes in all panels represent the intensity in the unit of Rayleigh.

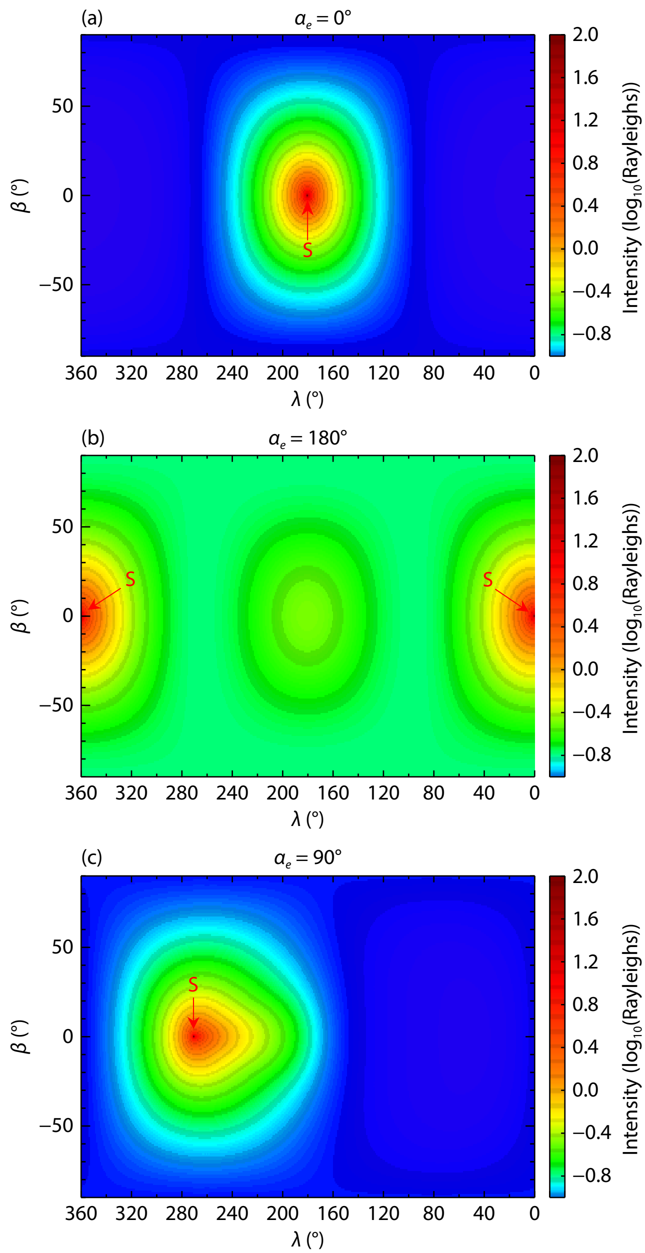

Figure 6. The all-sky maps of the 58.4 nm radiation intensity scattered by interstellar helium atoms, with the observer located on the Earth. Panel (a) shows the intensity where α_e = 0°, panel (b) where α_e = 180°, and panel (c) where α_e = 90°. The red arrows and "S" indicate the Sun. The horizontal and vertical axes represent the ecliptic longitude and latitude of the direction of the LOS, respectively (refer to Figure 1b for λ and β).

and the Sun–Earth line is denoted as α_e, and the distributions under three typical scenarios are taken into account in this section: where α_e = 0° (i.e. Earth is at the upwind axis), α_e = 180° (i.e. Earth is at the downwind axis), and where α_e = 90° (i.e. the Sun–Earth line is perpendicular to the symmetric axis).

Figure 4 presents the helium density distribution from the Earth's perspective. It clearly illustrates a sharp increase in densities around the focusing cone, regardless of Earth's location (that is, at any given time). In particular, when the Earth is positioned in the downwind axis, it can be observed that helium densities are rather high in any direction, with a peak density three times higher than that of interstellar helium atoms at infinity. Conversely, the lowest density appears in the upwind direction near the Sun, where the number of helium atoms can reduce to zero.

We rotated the density distribution in the ecliptic plane to gain the three-dimensional distribution of helium. The results were then substituted into the integral formula (Equation (8)), and we plotted the longitudinal and latitudinal scan of He I 58.4 nm radiation intensity, presented in Figure 5. In Figure 5, panels (a–c) show the longitudinal distribution of 58.4 nm radiation intensity, where α_e = 0° (a), α_e = 180° (b), α_e = 90° (c), and β = 0°; panels (d–f) show the latitudinal distribution from the ecliptic plane to the north ecliptic pole, where α_e = 0° (d), 180° (e), 90° (f), and λ = 70°. In Figure 5(a–c), for the case that T = 15,000 K, it can be found that the highest radiation intensity of 32.48 Rayleigh appears at α_e = 180° and λ = 0°, i.e. facing the upwind direction when the Earth is at the downwind axis; the lowest intensity of 0.19 Rayleigh appears when α_e = 0° and λ = 0°, i.e. facing the upwind direction when the Earth is at the upwind axis. Quantitatively, when the Earth moves into the helium focusing cone, i.e. every November to the following January, the intensity of 58.4 nm radiation scattered by interstellar helium atoms can reach 170 times that in the upwind zone (both when the LOS points to the upwind axis). In Figure 5(d–f), the intensity in the focusing cone (Figure 5e) is higher than that in other regions, and slightly decreases with an increase in latitude, while the others do the opposite.

We have considered the impact of varying the temperature of the ISW for α_e = 180° (Figure 5b and 5e), as the temperature effect significantly impacts the intensity near the downwind axis, while causing minor variation of intensity in other observation directions (Paresce and Bowyer, 1973). Figure 5b reveals that cooler ISW temperatures sharpen the peak intensity at λ = 180°, and elevate the intensity at the downwind axis (Figure 5b and 5e). This is consistent with the inference from Figure 2 and the findings in Paresce and Bowyer's Figure 6: the lower temperature of ISW results in a more compressive helium focusing cone with higher peak density and intensity at the downwind axis (Paresce and Bowyer, 1973). However, the effects of different solar line widths and Doppler shift are not considered in this paper. If we compare Figure 5(a–c) with Paresce and Bowyer's (1973) Figure 4, which considered solar line widths of 0.0015 nm and 0.015 nm, we find that the results of this work are not consistent with those in Paresce and Bowyer (1973) regarding a solar line width of 0.0015 nm, but they are similar in both qualitative and quantitative aspects with their results regarding a wider line of 0.015 nm. As pointed out by Paresce and Bowyer (1973), the use of a wider solar line causes a smoother intensity distribution, at the cost of some of the more distinctive features. Take the α_e = 180° case as an example, two prominent maximum intensities appearing at λ~60° and λ~300° (since the helium atoms are distributed symmetrically with the ISW direction as the axis) with a solar line width of 0.0015 nm completely disappear at that of 0.015 nm (Paresce and Bowyer, 1973). Additionally, if we compare Figure 5d with Paresce and Bowyer's (1973) Figure 7, it is evident that our result shows a smoother shape and a greater value. These discrepancies are expected, since our results neglecting the solar line width effect are more similar to those of Paresce and Bowyer

(1973) when applying a wider line.

When the ISW velocity is 20 km s^{-1} and the ISW temperature is 15,000 K, the range of the heliocentric radial velocity of helium atoms that causing the Doppler shift is v_{radial} = 0–20 km s^{-1}, and the thermal velocity of them is given by the most probable speed in the Maxwell–Boltzmann distribution: $v_{\mathrm{thermal}} = \sqrt{\frac{2kT}{m}} \approx 7.9$ km s^{-1}. The total effective velocity is their vector superposition, but for simplicity, a statistical superposition of the velocity amplitude (the Gaussian broadening model) is commonly used: $v_{\mathrm{total}} = |v_{\mathrm{radial}}| + |v_{\mathrm{thermal}}|$, ranging from 7.9 km s^{-1} to 29.9 km s^{-1}. According to the Doppler formula: $v_{\mathrm{Doppler}} = \frac{\Delta\lambda}{\lambda}c$, a wider solar line width of 0.015 nm corresponds to a Doppler velocity of 77.3 km s^{-1}, greater than the maximum total effective velocity, in which the solar line width completely covers the total absorption line broadening consists of the Doppler broadening and thermal broadening of helium atoms, thus the atoms can scatter effectively. Additionally, a narrower solar line width of 0.0015 nm corresponds to a Doppler velocity of 7.7 km s^{-1}, less than the minimum total effective velocity, in which the solar line width is unable to cover the total absorption line broadening, and the scattering efficiency is very low. When the solar line width is close to 0.015 nm, the spectra of the solar line and the helium absorption line overlap such that the influence of the solar line width and Doppler shift on the radiation intensity is relatively small. Therefore, our results which neglect the solar line width and the Doppler effect of neutral helium are nevertheless close to the results of Paresce and Bowyer (1973) using a wider solar line width of 0.015 nm, and it is an acceptable approximation to ignore these two effects in the calculation.

Based on the results shown in Figure 5, we obtain the expected all-sky maps of 58.4 nm radiation intensity observed from Earth where $\alpha_e = 0°$ (Figure 6a), 180° (b), and 90° (c). The results are shown in Figure 6. It can be observed that the closer the LOS is to the Sun, the greater the intensity becomes. This increase is due to the rapid rise in the g-factor. Notably, when the Earth is located on the downwind axis (see Figure 6b), the intensities along any LOS are higher than those when the Earth is at other positions in its orbital revolution (Figures 6a and 6c). In other words, for an observer at Earth, the sky in a 58.4 nm wavelength would be brighter in December than at any other time during the year. Our results are similar to Paresce and Bowyer's (1973) Figure 2, despite some minor discrepancies due to our neglecting of solar line width effect and applying a different set of interstellar parameters.

4. Discussion and Conclusions

Research into the interstellar medium and its interactions with the solar system is a key area of planetary physics. The solar EUV emission scattered by the neutrals in the interstellar wind provides an ideal opportunity to investigate the dynamic balance between the heliosphere and the surrounding interstellar environment, as well as the absorption and scattering effects of the interstellar medium on stellar EUV emissions, which are essential to the study of stellar EUV emissions.

In this work, we reviewed the previous modelling techniques used to describe the density distribution of interstellar helium atoms within the heliosphere and the corresponding 58.4 nm radiation intensity. We assumed that the velocity vector of the ISW direction is within the ecliptic plane, the distribution of helium atoms is cylindrically symmetrical with the ISW direction as the axis, and the atoms as collisionless free particles. We established models for both the density and radiation intensity distributions at different Earth orbital positions. Our findings indicate that, as the Earth enters the helium focusing cone in the downwind region, both the helium density and the 58.4 nm radiation intensity sharply increase. In fact, when situated on the Earth and facing the inflow direction of the interstellar wind, the radiation intensity in the downwind direction reaches up to 170 times that of the upwind direction. Given the pronounced gravitational focusing, and thus the enhancement in the temperature in the focusing cone, the temperature effect of the interstellar wind is significant and cannot be neglected. We found that the temperature affects the shape and features of the focusing cone, i.e. lower temperatures result in sharper and higher peak densities and intensities at the downwind axis.

However, for simplicity, this study omitted the effects of the solar line width and Doppler shift. Different solar line widths change the shape of the intensity profile, where a wider solar line results in a smoother shape with less distinctive features. The Doppler shift affects the absorption rate of solar lines by the interstellar atoms. Despite these limitations, our results are still innovative and offer advantages over previous results. In this study, we utilized a more reliable set of ISW parameters, rather than theoretical derivations only. The Queqiao-2 survey data, which has a much larger coverage in time and space than previous observations, will be included in the near future. Moreover, the contribution of the background radiation scattered by geocoronal helium, evident in observations from the Earth-orbited spacecraft EUVE (Vallerga et al., 2004), is absent in Queqiao-2's observations. This absence arises because Queqiao-2 operates in lunar orbit, which provides a vantage point largely unimpeded by geocoronal emission (Grava et al., 2018). Furthermore, the main purpose of our model is to facilitate Queqiao-2's EUV full-sky survey, which focuses on the EUV radiation from distant extrasolar stars, and is a frontier work in the world. By contrast, previous models were designed to study the interstellar environment in the neighborhood of the heliosphere. Therefore, our study provides new insights into the interstellar medium and its absorption effect on stellar EUV emissions, despite neglecting the effect of solar line width and Doppler shift.

Acknowledgments

We are grateful to Yixin Sun, Kaijun Liu, Jiansen He, Ziqi Wu, Hui Tian, Li Feng, and Zikang Xie for their insightful suggestions and guidance on this work. We also sincerely thank the two anonymous reviewers for their constructive comments and valuable suggestions that significantly improved the manuscript. This work is supported by the National Key R&D Program of China (2021YFA0718600) and the National Natural Science Foundation of China (42441809).

Supplementary Materials

Appendix A: Calculations on the Number Density of Interstellar Helium

A1 BPW's Modifications for Feldman's Approximation

The flaw in Feldman's approximation (Feldman et al., 1972) was modified by Blum et al., (1975) (i.e., the BPW model). The BPW team reanalyzed the helium density distribution along the downwind axis, assuming the interstellar gas outside the solar system has a Maxwellian velocity distribution, and ignoring the heating of interplanetary gas inside the heliosphere. They derived a form of integral that can be numerical integrated:

$$n(r,\pi)=N\int_{z_L}^{z_H}\exp\left[-\frac{z^2}{z+A}-\frac{r_e^2}{\tau_e r}\sqrt{\frac{m}{2kT}}\left(\pi-\frac{z}{\sqrt{z+A}}\frac{1}{V}\sqrt{\frac{2kT}{m}}\right)\frac{1}{\sqrt{z+A}}\right]\mathrm{d}z, \tag{A1}$$

with

$$A=\frac{GMm\,(1-\mu)}{rkT},$$

and the limits

$$z_{L,H}=\frac{m}{kT}V^2\left[1\pm\sqrt{1+\frac{2GM\,(1-\mu)}{rV^2}}\right].$$

The results of the two models were plotted in Figure A1, where panel (a) is duplicated from Blum et al. (1975), which shows both Feldman's approximation (dashed line) and BPW's modification (solid line). Our calculation using Feldman's approximation is shown in panel (b).

In the cases that (1) the mean thermal energy per atom is negligible compared to the mean translational energy per atom determined by V, and (2) the heliocentric distance considered is less than 50 AU, the Feldman approximation is applicable (Ajello, 1978). Therefore, we chose Feldman's approximation rather than BPW's modification to calculate the downwind density for simplicity.

A2 Johnson's Calculations

The radial and angular velocity components of helium atoms (u_r and u_θ, respectively) were derived as

$$u_r=\pm\sqrt{V^2+\frac{2\,(1-\mu)\,GM}{r}-\frac{p^2}{r^2}}, \tag{A2}$$

$$u_\theta=\frac{p}{r}, \tag{A3}$$

where p is the angular momenta of the two orbits:

$$p_1,p_2=\frac{1}{2}V\left[r\sin\theta'\pm\sqrt{r^2\sin^2\theta'+\frac{4r(1-\cos\theta')}{C}}\right], \tag{A4}$$

with the "plus" sign assigned to p_1 (the direct orbit) and the "minus" sigh assigned to p_2 (the indirect orbit). When $\mu<1$, $p_1>0$ and $p_2<0$. The angle θ' is the angle between the anti-direction of the inflow velocity of the ISW and the line between any point P and the Sun. The distribution of helium atoms in the heliosphere is cylindrically symmetrical with the direction of the ISW as the axis, and $|\sin\theta'|=\sin\theta$ ($0\le\theta\le\pi$ and $0\le\theta'\le 2\pi$).

According to Johnson (1972), one can derive the helium number density from the continuity equation, treating the trajectories as streamlines. Rewrite his result we obtain:

$$n\,(r,\theta)=\sum_{j=1}^{2}\frac{Nb_j^2\exp\left(\frac{-r_i\theta_j}{|b_j|}\right)}{r\sin\theta\sqrt{r^2\sin^2\theta+\frac{4r\,(1-\cos\theta)}{C}}}, \tag{A5}$$

with $b_j=p_j/V$, and $\theta_j=\theta$ if $p_j>0$, $\theta_j=2\pi-\theta$ if $p_j<0$. Note that the contribution of any trajectory that strikes the Sun before reaching point (r,θ) should be ignored (Johnson, 1972).

Johnson's formulae were recalculated in this paper (Figure A2). It is noticeable that the density near the downwind axis cannot be fully calculated, as it will be approaching infinity at the axis (a "singularity" appears). Therefore, Johnson's calculation is a less appropriate choice than the BPW model.

Appendix B: The Geometry of Helium Distribution

In order to obtain the helium distribution from the Earth's perspective (or from the vicinity of Earth), the two-dimensional heliocentric coordinates must be transformed into three-dimensional geocentric coordinates, i.e. the spherical ecliptic coordinates (r', λ, β). The three-dimensional distribution of helium atoms in the heliosphere can be easily obtained via rotating the planar distribution on the axis of the interstellar wind, as the flow direction of the wind forms an axis of symmetry for the distribution of interplanetary neutrals (Blum et al., 1975). Details are shown in Figure

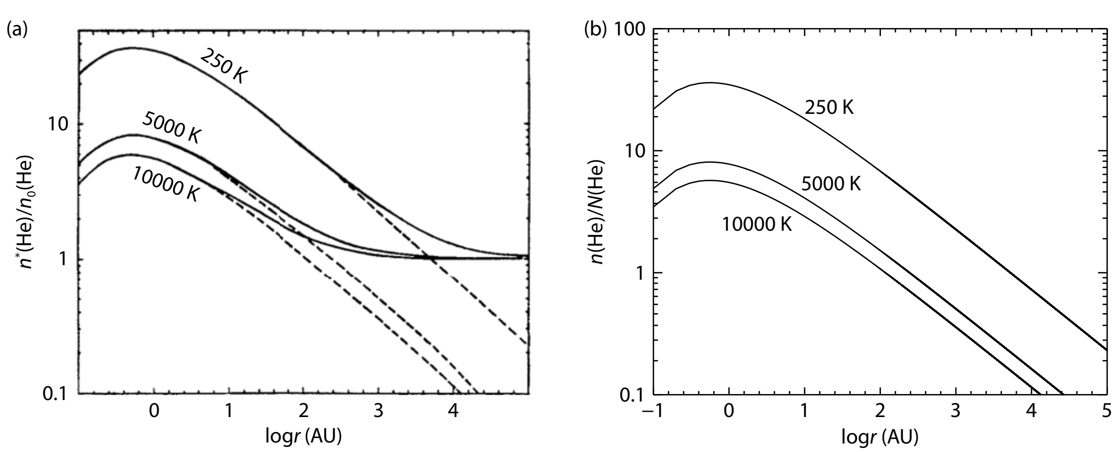

Figure A1. The relative helium number density along the downwind axis. Panels (a) and (b) represent the BPW result (Blum et al., 1975) and our result, respectively. The horizontal axis represents the heliocentric distance. The ISW parameters are V = 20 km/s, $\tau_e=1.5\times10^7$ s and T = 250 K, 5000 K, and 10,000 K.

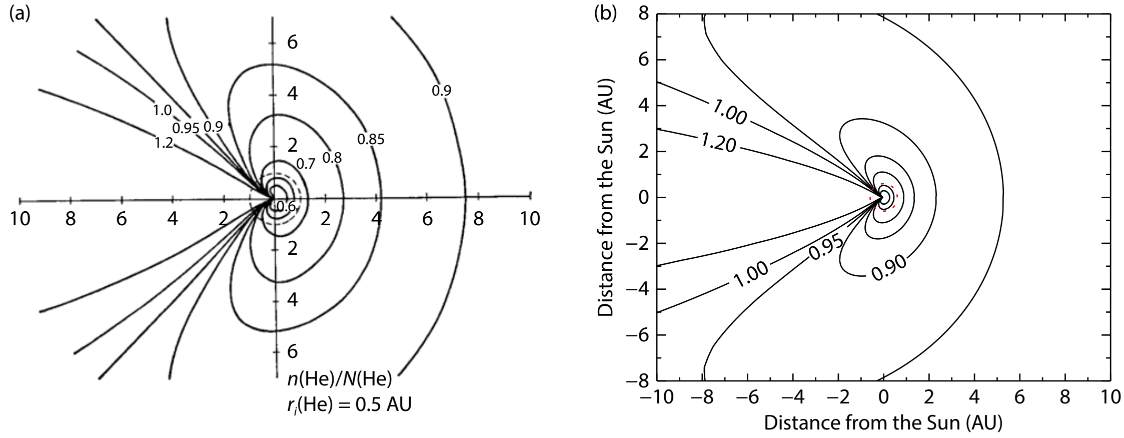

Figure A2. The relative helium number density in the ecliptic plane in a heliocentric polar coordinate system. Johnson's results (panel (a), Johnson, 1972) were re-presented in this paper (panel (b)). The dashed circles in both panels represent the Earth's orbit.

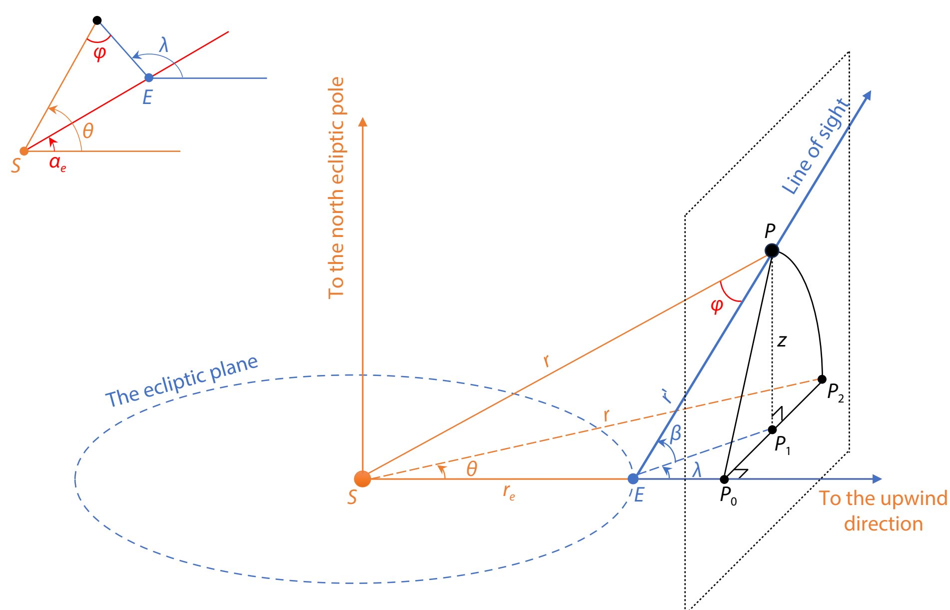

Figure B1. A diagram of the coordinate transitions. The heliocentric coordinates are shown as orange lines and letters, the geocentric coordinates are shown as blue lines and letters, and the letters "S", "E" and "P" represent the Sun, the Earth and the observing point, respectively. "P_0", "P_1" and "P_2" are in the ecliptic plane and the same plane as "P", which is perpendicular to the symmetric axis, with P_0 located in the upwind axis and $P_0P = P_0P_2$. In another word, P_2 is obtained by rotating P around the axis to the ecliptic plane, and the same value of helium density appears at the two points. The diagram draws the Earth on the upwind axis, and other positions are drawn in the upper left subplot, with α_e defined as the angle between the upwind direction and the Sun–Earth line, and φ defined as the polar phase angle of the scattering.

B1, note that the primary direction of the longitude here points from Earth to the anti-parallel direction of the ISW, instead of the vernal equinox.

In Figure B1, it can be easily seen that

$$z = r'\sin\beta,$$

$$SP_0 = r'\cos\beta\cos\lambda + r_e\cos\alpha_e,$$

$$P_0P_1 = r'\cos\beta\sin\lambda + r_e\sin\alpha_e,$$

$$P_0P_2 = P_0P = \sqrt{P_0P_1^2 + z^2},$$

and the heliocentric polar coordinates can be written as formulae of r', λ and β (for a fixed α_e):

$$\begin{cases} r = \sqrt{P_0P_2^2 + SP_0^2} = \sqrt{r'^2 + r_e^2 + 2r'r_e\cos\beta\cos(\lambda - \alpha_e)}, \\ \theta = \arccos\left(\dfrac{SP_0}{r}\right) = \arccos\left(\dfrac{r'\cos\beta\cos\lambda + r_e\cos\alpha_e}{r}\right). \end{cases} \quad \text{(B1)}$$

Thus, the problem of finding the density at point $P(r', \lambda, \beta)$ is converted into finding the density at point $P_2(r, \theta)$, which was given in Section 2.1. Note that if a two-dimensional transition is considered (e.g. convert heliocentric polar coordinate system to geocentric polar coordinate system in the ecliptic plane), then $\beta = 0$ in Equation (B1).

Appendix C: The Effects of the Solar Line Width and the Doppler Shift

The g-factor is the convolution of the solar line intensity with the

Doppler-shifted absorption cross section of the helium atoms and has been expressed analytically:

$$g(s) = g_e\left[\frac{r_e}{r(s)}\right]^2 \exp\left\{-\left[\frac{\Delta\lambda(s)}{\Delta\lambda_\tau}\right]^2\right\}, \tag{C1}$$

where $\Delta\lambda(s)$ is the Doppler shift from solar line center at position s, $\Delta\lambda_\tau$ is the square root of the sum of the squares of the thermal Doppler width and the solar line width (Ajello, 1978).

The 58.4 nm solar line is approximately in the shape of Gaussian line, with a full width at half-maximum (FWHM) of $122 \pm 2 \times 10^{-4}$ nm (Maloy et al., 1978). The FWHM of the resonant scattering cross section of the helium atoms far away from the solar system for a temperature of 15×10^3 K is about 15×10^{-4} nm, which is small compared with the solar line width (Ajello, 1978). Therefore, the exponential term in Equation (C1) can be ignored for a simpler calculation (Equation (11)) with a fixed solar line width and the Doppler effect neglected.

The effect of solar line width and the Doppler effect can be evaluated by taking the radial velocity distribution of the helium atoms into account, as the latter determines the rate of absorption of solar lines by the interplanetary gas (Wu FM and Judge, 1979). The radial velocity distribution of an interstellar gas has a Maxwell–Boltzmann (M-B) distribution of a radial temperature T_0, which can be simply evaluated by

$$T_0 = \frac{m}{2k}\left(\frac{V_{\frac{1}{2}}}{1.665}\right)^2, \tag{C2}$$

where $V_{1/2}$ is the FWHM of the radial velocity distribution. With the radial temperature for each observing point given, the absorption coefficient of the solar line can be further derived from

$$a_\nu = \frac{\pi e^2}{m_e c} f \frac{1}{\Delta\nu_0\sqrt{\pi}} \exp\left[-\frac{(\nu-\nu_0')^2}{\Delta\nu_0^2}\right], \tag{C3}$$

and

$$\nu_0' = \left(1 \pm \frac{u_r}{c}\right)\nu_0,$$

$$\Delta\nu_0 = \frac{\nu_0}{c}\sqrt{\frac{2kT_0}{m}},$$

are the shifted frequency and the Doppler broadening, respectively. In these equations, m_e is the electron mass, $f = 0.276$ is the oscillator strength of helium atoms, ν_0 is the frequency at the line center, and u_r is the radial velocity of the scattering atom.

The solar 58.4 nm flux at a point in photons cm^{-2} s^{-1} Hz^{-1} is given by

$$F_\nu = (\pi F_0)\left(\frac{r_e}{r}\right)^2 \frac{1}{\Delta\nu_s\sqrt{2\pi}} \exp\left[-\frac{\ln 2\left(\nu-\nu_0^2\right)}{2\Delta\nu_s^2}\right], \tag{C4}$$

where (πF_0) is the integrated solar flux at r_e and is set at a value of 8.9×10^8 photons cm^{-2} s^{-1} (Hall and Hinteregger, 1970), $\Delta\nu_s$ is the solar line FWHM. Hence the intensity of the scattered 58.4 nm radiation at 1 AU in Rayleigh is

$$I(\lambda,\beta) = 10^{-6} \times \int_0^\infty n(s)\, p[\varphi(s)] \int_0^\infty F_\nu a_\nu \mathrm{d}\nu \mathrm{d}s. \tag{C5}$$

Equation (C5) is equivalent to Equation (8), as the g-factor equals the integral $\int_0^\infty F_\nu a_\nu \mathrm{d}\nu$.

References

Ajello, J. M. (1978). An interpretation of mariner 10 helium (584 A) and hydrogen (1216 A) interplanetary emission observations. *Astrophys. J.*, *222*, 1068–1079. https://doi.org/10.1086/156224

Blum, P. W., Pfleiderer, J., and Wulf-Mathies, C. (1975). Neutral gases of interstellar origin in interplanetary space. *Planet. Space Sci.*, *23*(1), 93–105. https://doi.org/10.1016/0032-0633(75)90070-7

Craig, N., Abbott, M., Finley, D., Jessop, H., Howell, S. B., Mathioudakis, M., Sommers, J., Vallerga, J. V., and Malina, R. F. (1997). The *extreme ultraviolet explorer* stellar spectral atlas. *Astrophys. J. Suppl. Ser.*, *113*(1), 131–193. https://doi.org/10.1086/313052

Drake, J. J., Kashyap, V. L., Wargelin, B. J., and Wolk, S. J. (2020). Pointing Chandra toward the extreme ultraviolet fluxes of very low mass stars. *Astrophys. J.*, *893*(2), 137. https://doi.org/10.3847/1538-4357/ab7b5c

Feldman, W. C., Lange, J. J., and Scherb, F. (1972). Interstellar helium in interplanetary space. In Solar Wind. C. P. Sonett et al. (Eds.), *Nasa Special Publication*, SP-308, p. 684.

Frisch, P. C. (2006). *Solar Journey: The Significance of Our Galactic Environment for the Heliosphere and Earth*. Dordrecht: Springer Netherlands. https://doi.org/10.1007/1-4020-4557-3

Frisch, P. C., Bzowski, M., Livadiotis, G., McComas, D. J., Moebius, E., Mueller, H. R., Pryor, W. R., Schwadron, N. A., Sokół, J. M., … Ajello, J. M. (2013). Decades-Long changes of the interstellar wind through our solar system. *Science*, *341*(6150), 1080–1082. https://doi.org/10.1126/science.1239925

Frisch, P. C., Bzowski, M., Drews, C., Leonard, T., Livadiotis, G., McComas, D. J., Möbius, E., Schwadron, N., and Sokół, J. M. (2015). Correcting the record on the analysis of *IBEX* and *STEREO* data regarding variations in the neutral interstellar wind. *The Astrophysical Journal*, *801*(61), https://doi.org/10.1088/0004-637X/801/1/61

Gloeckler, G., Cain, J., Ipavich, F. M., Tums, E. O., Bedini, P., Fisk, L. A., Zurbuchen, T. H., Bochsler, P., Fischer, J., … Kallenbach, R. (1998). Investigation of the composition of solar and interstellar matter using solar wind and pickup ion measurements with SWICS and SWIMS on the ace spacecraft. In C. T. Russell, et al. (Eds.), *The Advanced Composition Explorer Mission* (pp. 497–539). Dordrecht: Springer. https://doi.org/10.1007/978-94-011-4762-0_18

Grava, C., Pryor, W. R., Feldman, P. D., Retherford, K. D., Gladstone, G. R., and Greathouse, T. K. (2018). LRO/LAMP study of the interstellar medium via the HeI 58.4 nm resonance line. *Astron. Astrophys.*, *616*, A159. https://doi.org/10.1051/0004-6361/201731555

Hall, L. A. and Hinteregger, H. E. (1970). Solar radiation in the extreme ultraviolet and its variation with solar rotation. *Journal of Geophysical Research*, *75*(34), 6959–6965. https://doi.org/10.1029/JA075i034p06959

He, F., He, L. P., Chen, B., Zhang, X. X., Guo, Q. F., Han, Z. W., Wang, X. D., Wang, H. F., Zhang, H. J., … Wang, C. (2025). Dual-wavelength extreme ultraviolet camera (EUC) for the Chang'E-7 mission: Scientific objectives and system design. *Sci. China Technol. Sci.*, *68*, 2100601 (2025). https://doi.org/10.1007/s11431-024-2838-4

He, L. P., He, F., Chen, B., Zhang, X. X., Guo, Q. F., Han, Z. W., Wang, X. D., Zhang, H. J., Mao, S. L., … Wang, C. (2025). Dual-wavelength extreme ultraviolet camera (EUC) for the Chang'E-7 mission: Instrument development and calibration. *Sci. China Technol. Sci.*, *68*, 2220601 (2025). https://doi.org/10.1007/s11431-024-2839-x.

Johnson, H. E. (1972). Backscatter of solar resonance radiation—I. *Planet. Space Sci.*, *20*(6), 829–840. https://doi.org/10.1016/0032-0633(72)90168-7

Johnstone, C. P., Bartel, M., and Güdel, M. (2021). The active lives of stars: A complete description of the rotation and XUV evolution of F, G, K, and M dwarfs. *Astron. Astrophys.*, *649*, A96. https://doi.org/10.1051/0004-6361/202038407

Kubiak, M. A., Bzowski, M., Sokół, J. M., Swaczyna, P., Grzedzielski, S., Alexashov, D. B., Izmodenov, V. V., Möbius, E., Leonard, T., … McComas, D. J. (2014). Warm breeze from the starboard bow: a new population of neutral helium in the heliosphere. *Astrophys. J. Suppl. Ser.*, *213*(2), 29. https://doi.org/10.1088/0067-0049/213/2/29

Lallement, R., and Bertaux, J. L. (2014). On the decades-long stability of the interstellar wind through the solar system. *Astron. Astrophys.*, *565*, A41. https://doi.org/10.1051/0004-6361/201323216

Maloy, J. O., Carlson, R. W., Hartmann, U. G. and Judge, D. L. (1978). Measurement of the profile and intensity of the solar He I λ584-Å resonance line. *Journal of Geophysical Research: Space Physics*, *83*(A12), 5685−5690. https://doi.org/10.1029/JA083iA12p05685

McComas, D. J., Bzowski, M., Fuselier, S. A., Frisch, P. C., Galli, A., Izmodenov, V. V., Katushkina, O. A., Kubiak, M. A., Lee, M. A., … Wurz, P. (2015). Local interstellar medium: six years of direct sampling by *IBEX*. *Astrophys. J. Suppl. Ser.*, *220*(2), 22. https://doi.org/10.1088/0067-0049/220/2/22

Möbius, E., Hovestadt, D., Klecker, B., Scholer, M., Gloeckler, G., and Ipavich, F. M. (1985). Direct observation of He^+ pick-up ions of interstellar origin in the solar wind. *Nature*, *318*(6045), 426–429. https://doi.org/10.1038/318426a0

Nakagawa, H., Bzowski, M., Yamazaki, A., Fukunishi, H., Watanabe, S., Takahashi, Y., Taguchi, M., Yoshikawa, I., Shiomi, K., and Nakamura, M. (2008). UV optical measurements of the Nozomi spacecraft interpreted with a two-component LIC-flow model. *A&A*, *491*(1), 29−41. https://doi.org/10.1051/0004-6361:20079241

Paresce, F., and Bowyer, S. (1973). Resonance scattering from interstellar and interplanetary helium. *Astron. Astrophys., 27*, 399−406.

Paresce, F., Bowyer, S., and Kumar, S. (1973). Evidence for an interstellar or interplanetary source of diffuse He I 584 Å radiation. *Astrophys. J.*, *183*, L87. https://doi.org/10.1086/181258

Rucinski, D., and Fahr, H. J. (1989). The influence of electron impact ionization on the distribution of interstellar helium in the inner heliosphere-possible consequences for determination of interstellar helium parameters. *Astron. Astrophys.*, *224*(1-2), 290–298.

Spitzer, S. A., Lepri, S. T., Raines, J. M., Gilbert, J. A., Bower, J., Dewey, R. M., and Möbius, E. (2024). Determining the interstellar wind longitudinal inflow evolution using pickup ions in the helium focusing cone. *Astrophys. J.*, *974*(1), 87. https://doi.org/10.3847/1538-4357/ad6868

Swaczyna, P., Bzowski, M., Heerikhuisen, J., Kubiak, M. A., Rahmanifard, F., Zirnstein, E. J., Fuselier, S. A., Galli, A., McComas, D. J., … Schwadron, N. A. (2023). Interstellar conditions deduced from interstellar neutral helium observed by IBEX and global heliosphere modeling. *Astrophys. J.*, *953*(1), 107. https://doi.org/10.3847/1538-4357/ace719

Thomas, G. E. (1978). The interstellar wind and its influence on the interplanetary environment. *Ann. Rev. Earth Planet. Sci*, *6*(1): 173−204. https://doi.org/10.1146/annurev.ea.06.050178.001133

Vallerga, J., Lallement, R., Lemoine, M., Dalaudier, F., and McMullin, D. (2004). EUVE observations of the helium glow: Interstellar and solar parameters. *Astron. Astrophys.*, *426*(3), 855–865. https://doi.org/10.1051/0004-6361:20035887

Witte, M., Rosenbauer, H., Keppler, E., Fahr, H., Hemmerich, P., Lauche, H., Loidl, A., and Zwick, R. (1992). The interstellar neutral-gas experiment on ULYSSES. *Astron. Astrophys. Suppl. Ser.*, *92*, 333–348.

Witte, M. (2004). Kinetic parameters of interstellar neutral helium: Review of results obtained during one solar cycle with the Ulysses/GAS-instrument. *Astron. Astrophys.*, *426*(3), 835–844. https://doi.org/10.1051/0004-6361:20035956

Wu, F. M., and Judge, D. L. (1979). Temperature and flow velocity of the interplanetary gases along solar radii. *Astrophys. J.*, *231*, 594–605. https://doi.org/10.1086/157221